15 Computer Assisted Physics

P. F. Meier, S. Dangel, P. Hüsser, H. R. Moser, Y. Shen and J. M. Singer

15.1 Introduction

The Computer Assisted Physics group has continued its research activities in computational physics. Selected examples of progress are presented in the following subsections. They comprise (i) investigations of the electronic structure of materials exhibiting high-temperature superconductivity using large-scale cluster calculations and (ii) Quantum Monte-Carlo calculations of the susceptibilities of the anisotropic antiferromagnetic Heisenberg model. Furthermore, (iii) we report on the activities in the analysis of nonlinear dynamical systems, a project which is pursued in the frame of a collaboration with the department for Neurology of the University Hospital. Finally, (iv) investigations of molecular wave phenomena in porous media, that are performed in collaboration with a private company, are presented.

15.2 Electronic structure calculations of high-temperature superconductors

The electronic structure of high$-T_c$ materials has been investigated with density functional calculations within the local density approximation (LDA) [1]. These calculations do provide information about the ground state charge density distribution and hybridization parameters, but they reproduce neither the semiconducting behavior of La_2CuO_4 nor the magnetic properties of the ground state.

The cluster method supplements the results of band-structure calculations. It has the advantage that correlation effects can - at least in principal - be accounted for by configuration interaction (CI) procedures. Furthermore, it is possible to go beyond LDA by generalized gradient approximations (GGA). The most serious disadvantage is the finite size of the clusters that can numerically be treated. Therefore, the influence of the surrounding ions has to be taken into account by adjusting the correct Madelung potential in the central region of the cluster.

The quality of electronic structure calculations can be tested by studying the electric field gradients (EFGs) at various nuclear sites. The EFGs depend sensitively on the charge distribution and thus provide information about the ground state. Their values have been determined experimentally by NMR and NQR for a variety of nuclei in the high$-T_c$ materials [2].

Theoretical approaches [3, 4] give EFG values that, apart from one exception, more or less agree with the experimental data. The exceptional case is the EFG at the planar Cu(2) site in the $YBa_2Cu_3O_n$ compounds. In the past two years we have applied the cluster approach to study the electronic structure of $YBa_2Cu_3O_7$. The focus was on the evaluation of the EFG's at the Cu sites. Using a rather large cluster (comprising 12 Cu and 42 O, as well as 12 Y and 8 Ba atoms) which was furthermore embedded in a lattice of more than 2000 point charges, we calculated the electronic structure with three different methods: Hartree-Fock (HF), LDA and GGA [5, 6]. For LDA and GGA calculations, the EFGs at the Cu(2) site are much closer to the experimental values ($V_{zz} = 12.3 \times 10^{21}$ Vm^{-2}) than those obtained with other theoretical approaches [3, 4]. Furthermore, by simulating the change of lattice sites upon applying hydrostatic pressure, we were able to reproduce the measured relative change of the quadrupolar frequency ν_Q which is proportional to V_{zz} rather well as is shown in Fig. 15.1.

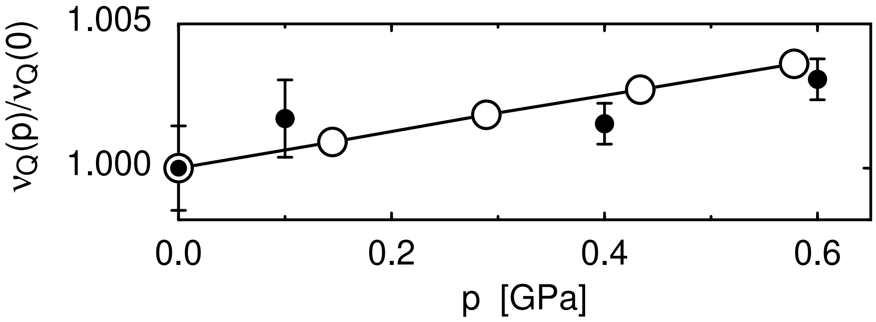

Figure 15.1: Normalized pressure dependent NQR frequencies $\nu_Q(p)/\nu_Q(0)$ for Cu(2) in $YBa_2Cu_3O_7$.• experiments [7]. ○ our densitiy functional calculations (GGA) [8].

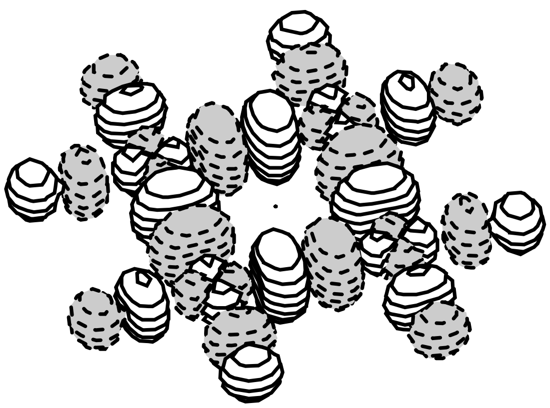

Figure 15.2: Highest occupied molecular orbital in the cluster Cu_4O_{20}/Cu_8La_{26}. The shadowed regions indicate negative sign of the corresponding atomic wave functions.

First spin-polarized studies have also been performed for the La_2CuO_4 structure with different clusters: (i) CuO_6/Cu_4La_{10} where one Cu and six O atoms were treated in an all electron basis while for additional 4 Cu and 10 La atoms pseudopotentials were used and (ii) Cu_4O_{20}/Cu_8La_{26}. For the latter, Fig. 15.2 depicts the highest occupied molecular orbit (HOMO) obtained with GGA calculations. There is a strong antibonding hybridization between the Cu $3d_{x^2-y^2}$ (33 %) and the O $2p_x$ and $2p_y$ (67 %) atomic orbitals. The corresponding quadrupole frequencies at the Cu site are given in Table 15.1. Again, the values obtained with the density functional method with GGA compare well with the experimental data.

method	HF	HF	HF	GGA	GGA	
Ref.	[9]	[10]	present	present	present	exp.
cluster	CuO_6	CuO_6	CuO_6/Cu_4La_{10}	CuO_6/Cu_4La_{10}	Cu_4O_{20}/Cu_8La_{26}	
ν_Q	47	39	48	35	34	33

Table 15.1: ^{63}Cu NQR frequencies (MHz) for La_2CuO_4.

15.3 Quantum Monte-Carlo simulations of the antiferromagnetic Heisenberg model

Following the discovery of high-temperature superconductors the two-dimensional spin-$\frac{1}{2}$ antiferromagnetic Heisenberg model has received much attention since there are experimental indications that spin dynamics plays an important role in the new superconducting mechanisms. Copper spins in Cu-O planes of the undoped compound La_2CuO_4 exhibit strong two dimensional antiferromagnetic correlation, which is reasonably well described by the Heisenberg model. In this work we have studied one-dimensional antiferromagnetic Heisenberg models over a wide range of anisotropy via a large-scale quantum Monte-Carlo (QMC) simulation [11]. These models are described by the generalised Hamiltonian:

$$\mathcal{H} = J \sum_i \left\{ S_i^x S_{i+1}^x + S_i^y S_{i+1}^y + a \cdot S_i^z S_{i+1}^z \right\}, \tag{15.1}$$

where $\vec{\mathcal{S}}_i = (S_i^x, S_i^y, S_i^z)$ is the spin operator at the i-th site and the parameter a represents the anisotropy in z-direction. The energy scale is set by the exchange coupling J. In this work we have implemented both the conventional worldline algorithm and the modern loop algorithm [12]. The latter can improve the performance of the QMC simulation by orders of magnitude. Using these methods, we have calculated the finite-temperature susceptibilities shown in Fig. 15.3. Our QMC-results are represented by different symbols, which are connected by dotted lines. The bold solid lines are analytical results for some special cases of the Heisenberg model. We found good agreements between the QMC simulations and the analytical results for $a = 0$ (XY model) and $a = 1$ (isotropic case). In the high-temperature region all $\chi(T)$-curves converge to the Curie law. The deviations at low temperature indicate the quantum nature of spin-$\frac{1}{2}$ systems. In contrast to other cases, in the Ising-like region ($a > 1$) a finite susceptibility at zero temperature does not exist. This indicates an energy gap between the ground state and excited states which is due to the existence of an anisotropy. The experience gained with the solutions for the one-dimensional system may facilitate the application of the QMC-simulation to two- and three-dimesional systems.

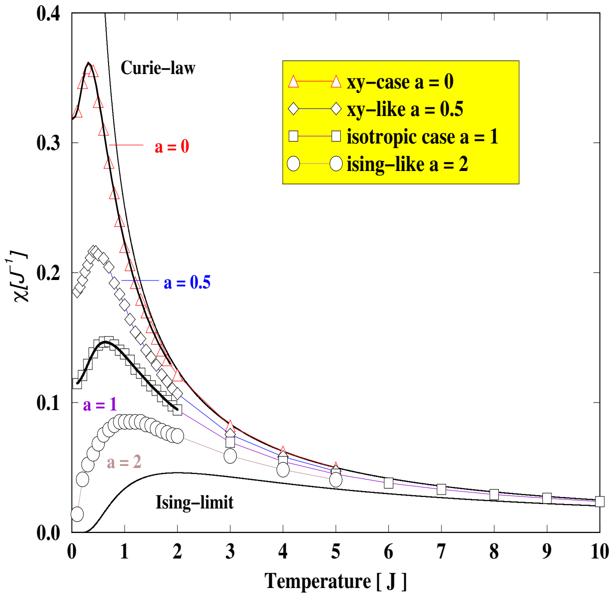

Figure 15.3: Temperature dependence of the susceptibility in the one-dimensional antiferromagnetic Heisenberg model calculated with QMC for various anisotropy values a. The solid lines for $a = 0, 1$, and ∞ (Ising model) are analytical results.

15.4 Electroencephalograms in epilepsy: analysis and seizure prediction within the framework of Lyapunov theory

Epileptic seizures are defined as the clinical manifestation of excessive and hypersynchronous activity of neurons in the cerebral cortex and represent one of the most frequent malfunctions of the human central nervous system. Therefore, the search for precursors and predictors of a seizure is of utmost clinical relevance and may even guide us to a deeper understanding of the seizure generating mechanisms.

It has been known for a long time that seizure prediction cannot be based only on the density of visible epileptiform patterns in the electroencephalogram (EEG). However, some of the analysis methods within the field of nonlinear dynamics are sensitive to "hidden" properties of a signal: There exist chaos–indicators that well have the discrimination power between the so–called preictal signals (i.e., a few minutes prior to a seizure onset) and the interictal ones.

We extracted complexity measures such as Lyapunov exponents and Kolmogorov entropies from intracranial EEGs (invasive and semi–invasive methods) that mainly originate from the group around Prof. H. G. Wieser at the University Hospital Zurich, but also from a group around Prof. C. E. Elger at the University Hospital in Bonn. Among the computational methods we tested so far, we find that the spectral density of the local expansion exponents is best suited to predict the onset of a forthcoming seizure. Our results on this matter are summarized in quite some detail in Ref. [13].

Below we concentrate on a somewhat different issue, namely we aim at a critical assessment of the question whether the deterministic share in an EEG can be quantified. This question is not an easy one, particularly since a high–dimensional noisy time series necessarily must be filtered, which then alters also the underlying "true" signal. We investigated a 64 channel EEG from a subdural 8 by 8 grid–electrode, i.e., a recording technique that generally provides particularly "clean" and stationary signals. The patient suffers from a so–called frontal lobe epilepsy. We prefer to use multichannel reconstruction, since this type of analysis proves a significantly lower noise sensitivity compared to the delay–embedding technique. Fig. 15.4 displays two Lyapunov spectra, i.e., as many Lyapunov exponents as phase space

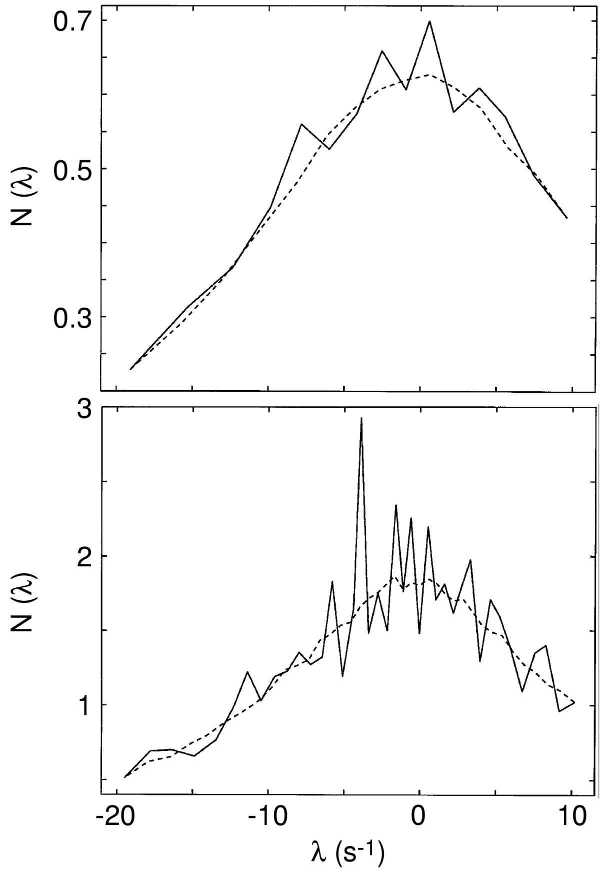

Figure 15.4: Lyapunov spectra, i.e., as many Lyapunov exponents as phase space dimensions, represented as a spectral density. The EEG data originating from an 8 by 8 subdural grid–electrode were used. Top: rows 1 and 2 in the grid, i.e., 16 phase space dimensions. Bottom: rows 1 through 5, i.e., 40 dimensions. We prefer to see $N(\lambda)$ as a dimensionless number of events, although its construction implies units of seconds. For an increasingly large number of phase space dimensions, this representation exhibits the convergence of the Lyapunov spectra.

dimensions, represented as spectral densities. The solid curves are given by the reciprocal distances between adjacent exponents. Clearly such spectra look rather toothed, since a minute variation in the small distances gets strongly amplified in their reciprocal values. The dashed curves emerge from a smoothening procedure based on a "centre of mass"–approach, i.e., the intensities are made up from several Lyapunov exponents used at a time.

A bunch of similar plots reveals that we achieve convergence in the range of, say, 10 up to 12 phase space dimensions. We cannot commit ourselves to an exact number, since this depends somewhat on the applied criteria. In particular, one might focus on the largest and smallest exponents only. The convergence of such spectra is in strict disagreement with a stochastic behavior, thus it exhibits the deterministic properties of the underlying signal.

We are aware that other EEG–recording techniques are attended with much higher noise levels. Nevertheless we think that our results provide an important step towards a quantitatively correct characterization of such signals: Most approaches are based on a given number of phase space dimensions. Therefore it appears desirable to know initially whether the chosen size of the phase space is sufficient.

15.5 Nonlinear wave phenomena in porous media

Recent advances in ultra high sensitive seismic detector technology allow for the direct measurement of even very weak nonlinear seismic signals. The company ADNR Technology Sagl, situated in Minusio, Ticino, has been able to observe such an effect which depends on the fluid saturation of a porous layer. This technology can be used as a direct indicator for oil, gas and water content. Fig. 15.5 shows the spectra of the seismic wave originating from an oil reservoir several km deep as observed at the surface. A peak at about 3 Hz occurs at locations where the oil content is still high, while the signal at depleted locations is flat. ADNR has been able to reproducibly measure this effect and the correlation with the well known oil distribution of the reservoir is very good.

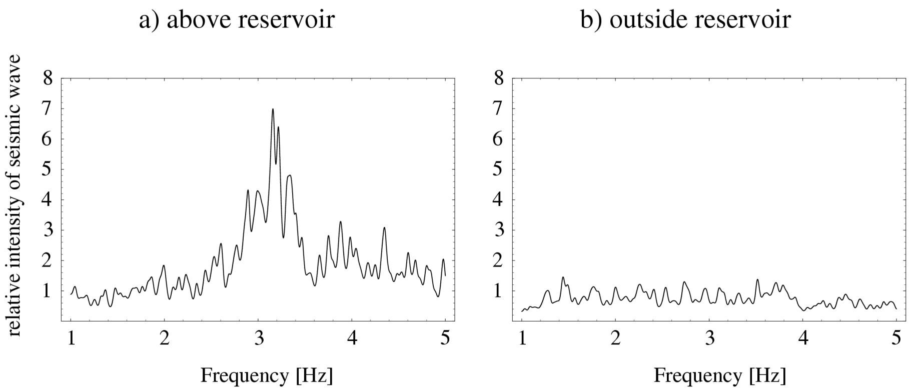

Figure 15.5: Experimental data from an oil field. a) corresponds to a point situated directly above the reservoir. b) corresponds to a point situated outside the border of the reservoir.

To this date there exists no established theory about the origins of this effect. In order to develop a theoretical explanation, we are considering

- autowaves, feedback and memory mechanisms in porous media [14],
- scattering and reflection of waves in layered media [15],
- nonlinear wave propagation mechanisms, wave modulation [16],
- nonlinear oscillations of fluids in porous media [17],
- non-Newtonian fluid flow behavior (thixotropy, Knudsen flow) [18],

Our current model consists of an autowave process based on a nonlinear pore mechanism and driven by global flux in the reservoir. It can explain the occurrence of the low frequency peak, but has not yet been developed far enough to give quantitative results.

References

[1] for a review, see K. C. Haas, Solid State Physics, Vol. 42 ed. by H. Ehrenreich and D. Turnbull (1989).

[2] for a review, see D. Brinkmann and M. Mali, in NMR – Basic Principles and Progress, ed. P. Diehl et al., Vol. 31, p 171 (1994).

[3] K. Schwarz et al., Phys. Rev. B **42**, 2051 (1990).

[4] N. Sahoo et al., Phys. Rev. B **41**, 220 (1990).

[5] H. U. Suter, E. P. Stoll, P. Hüsser, S. Schafroth, and P. F. Meier, Physica C, **282-287**, 1639 (1997).

[6] P. Hüsser, E. Stoll, H. U. Suter, P. F. Meier, Physica C, **294**, 217 (1998).

[7] K. Müller, M. Mali, J. Roos, and D. Brinkmann, Physica C, **162-164**, 173 (1989).

[8] P. Hüsser, S. Schafroth, E. Stoll, H. U. Suter, and P. F. Meier, Helv. Phys. Acta, **70**, Separanda 2, S25 (1997).

[9] S. B. Sulaiman, N. Sahoo, T. P. Das, O. Donzelli, E. Torikai, and K. Nagamine, Phys. Rev. B **44**, 7028 (1991).

[10] R. L. Martin, Phys. Rev. Lett., **75**, 744 (1995).

[11] M. S. Makivic and Hong-Qiang Ding, Phys. Rev. B **43**, 3562(1991);

[12] H.G. Evertz, The Loop Algorithmus. In Numerical Methods for Lattice Quantum Many-Body Problems, D. J. Scalapino, Addison Wesley Longman, Frontiers in Physics.

[13] H. R. Moser, B. Weber, H. G. Wieser, and P. F. Meier, Physica D, in press.

[14] V. A. Vasiliev, in *Autowave processes in kinetic systems.* Reidel, 1990.

[15] L. M. Brekhovskikh and O. A. Godin, *Acoustics of layered media I and II.* Springer, 1990.

[16] I. Ya. Edelman, Propagation of nonlinear waves in a porous medium with two-phase saturation by a liquid and a gas. *Fluid Dynamics (Moscow)*, **31**, 552, (1996).

[17] S. Martin, A hydrodynamic curiosity: the salt oscillator. *Geophysical Fluid Dynamics (GB)*, **1**, 143, (1970).

[18] R. Meyer and F. F. Krause, Experimental evidence for permeability minima at low-velocity gas flow through naturally formed porous media. *J. Porous Media*, **1**, 93, (1998).